Beyond the Born-Oppenheimer static surface model for molecule-surface reactions

Spiering, P.

Chapter 4

Testing Electronic Friction Models: Vibrational De-excitation in Scattering of H_2 and D_2 on Cu(111)

This chapter is based on P. Spiering and J. Meyer. "Testing Electronic Friction Models: Vibrational De-Excitation in Scattering of H_2 and D_2 from Cu(111)". In: *J. Phys. Chem. Lett.* 9 (2018), pp. 1803–1808.

Abstract

At present, molecular dynamics with electronic friction (MDEF) is *the* workhorse model to go beyond the Born-Oppenheimer approximation in modeling dynamics of molecules at metal surfaces. Concomitant friction coefficients can be calculated with either the local density friction approximation (LDFA) or orbital-dependent friction (ODF) which – unlike LDFA – accounts for anisotropy while relying on other approximations. Due to the computational cost of ODF, extensive high-dimensional MDEF trajectory calculations of experimentally measurable observables have hitherto only been performed based on LDFA. In order to overcome this limitation a continuous neural-network-based representation has been constructed for the scattering of vibrationally excited H_2 and D_2 from Cu(111). An up to three times higher vibrational de-excitation probabilities is predicted with ODF compared to LDFA. These results indicate that anisotropic electronic friction can be important for specific molecular observables. Future experiments can test for this "fingerprint" of different approximations underlying state-of-the-art MDEF.

4.1 Introduction

The motion of atomic and molecular adsorbates on metal surfaces underlies every elementary reaction steps in heterogeneous catalysis. Due to the absence of an energy gap between valence and conduction band electrons, these motions can result in the excitation of electron-hole pairs (ehps) and thus violate the Born-Oppenheimer approximation [2–4]. A growing number of experiments points to the importance of this non-adiabatic energy loss channel [5]. On the other hand, the development of suitable theoretical models to account for these non-adiabatic effects is still an ongoing process [6–10]. For systems with weak non-adiabatic coupling, molecular dynamics with electronic friction (MDEF)[11] is currently the most popular approach [12]. MDEF relies on a potential energy surface (PES) nowadays typically obtained from density functional theory (DFT)[4], and accounts for the effects of the ehps on the motion of the nuclei by electronic friction coefficients [11]. One state-of-the-art technique for cal-

culating these coefficients as functions of the adsorbate positions relies on mapping to an atom-in-jellium model for which only the surface electron density is considered (local density friction approximation, LDFA[13, 14]). Alternatively, the electronic states of the molecule-surface system can be taken into account (orbital-dependent friction, ODF[11, 15]). For the inelastic scattering of H atoms from Au(111), millions of MDEF trajectories based on a high-dimensional PES[16] and local density friction approximation (LDFA) have recently been demonstrated to yield accurate scattering probabilities in excellent agreement with experimental data [17].

The situation is quite different for molecules. Due to its combination with the independent atom approximation, the LDFA completely neglects any molecular effects [13]. Orbital-dependent friction (ODF) on the other hand accounts for the anisotropic tensorial character of friction coefficients on corrugated metal surfaces and along adsorbate-internal bonds [18–20], which is why ODF has been argued to be "theoretically" more accurate for (diatomic) molecules [21]. However, this discussion [13, 21, 22] has still remained inconclusive, because an evaluation of ODF comes at very high computational costs. Consequently, extensive MDEF trajectory calculations for molecules including all relevant degrees of freedom (DOF) can be easily performed with LDFA[12, 13], whereas only two molecular DOF have so far been included for ODF[23]. The very recent on-the-fly evaluation of ODF within *ab initio* molecular dynamics by [20] is an important step, but the less than 20 calculated trajectories make direct validation via molecular beam experiments impossible. Modeling the non-adiabatic contribution to vibrational lifetimes of molecules adsorbed on metal surfaces on the other hand does not require such extensive statistical averaging [24, 25]. The most recent implementations of LDFA and ODF both yield results that agree with experimental data within the error bars [26, 27]. Furthermore, Novko *et al.* have shown recently in this context [28] that the numerical evaluation of friction tensors within ODF [20, 27] effectively includes potentially spurious electronic memory effects with unclear consequences for MDEF[29]. Given this situation, theoretical understanding and modeling relying on MDEF faces an important question: Is the molecular anisotropy as described by ODF important for any observables that can be validated by high-precision molecular beam

experiments like for atoms [17]?

The work in this chapter provides an answer to this question using H_2 and D_2 on Cu(111). For this system, the weak non-adiabatic coupling as well as static surface approximation are well justified [30–32], and an accurate DFT-based PES relying on the semi-empirically constructed specific reaction parameter (SRP) exchange-correlation functional is available [33, 34]. A six-dimensional neural-network-based continuous representation of ODF has been constructed that allows for extensive MDEF trajectory calculations on equal footing with LDFA. While dissociative sticking probabilities are hardly affected in general and by the type of electronic friction coefficients used, vibrational de-excitation probabilities are argued to be a "fingerprint", which can be used to distinguish and validate LDFA and ODF in future experiments, in this chapter.

4.2 Methods

In this section an extension of Chap. 2 is given for the methods used specifically in this chapter.

4

4.2.1 Molecular Dynamics with Electronic Friction and the Potential Energy Surface

Quasi-classical trajectory calculations [33] within MDEF rely on a generalized Langevin equation [11]

$$m_i \frac{d^2 R_{i\alpha}}{dt^2} = -\frac{\partial V(\mathbf{R})}{\partial R_{i\alpha}} - \underbrace{\sum_{j=1}^{N}\sum_{\beta=1}^{3} \eta_{i\alpha j\beta}\dot{R}_{j\beta}(\mathbf{R})}_{F_{i\alpha}^{\mathrm{fric}}(\mathbf{R})} + \mathcal{F}_{i\alpha}(t), \tag{4.1}$$

where i, j indicate atoms and α, β Cartesian coordinates. Atomic masses and positions are denoted by m_i and $\mathbf{R}_i$, respectively. For a H_2 or D_2 molecule on a static surface, the total number of moving atoms N is two resulting in six DOF. In addition to the forces from the PES $-\frac{\partial V(\mathbf{R})}{\partial R_{i\alpha}}$, which yield the adiabatic dynamics, non-adiabatic effects on the nuclear dynamics originate from electronic friction forces $F_{i\alpha}^{\mathrm{fric}}(\mathbf{R})$ and thermal

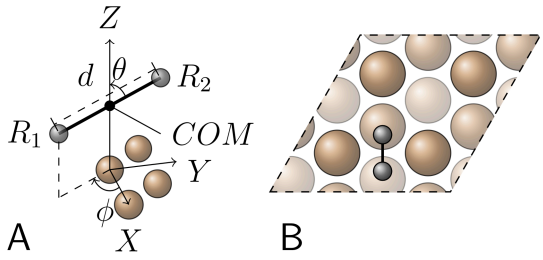

Figure 4.1: A) Molecular coordinate system denoting the center of mass positions (X, Y, Z), bond length d as well as spherical orientation (θ, ϕ). B) Top view of a reference configuration with $X = \frac{1}{2}a$, $Y = 0$ and $\theta_0 = \phi_0 = 90°$ from the minimum energy reaction path for dissociative chemisorption over the bridge site [35], where a denotes the surface lattice constant. Cu atoms in the first, second and third layer are depicted by increasing transparence. Note that $X, Y, Z = 0$ corresponds to the position of a Cu atom in the surface plane (top site).

white noise $\mathcal{F}_{i\alpha}(t)$, respectively. In this work, $V(\mathbf{R})$ is mainly taken to be the static surface PES based on the SRP48 exchange-correlation functional from Ref. [34], but dynamics calculations have also been performed and compared with the PW91-PES from earlier work [35]. The friction forces are linear in nuclear velocities $\dot{R}_{j\beta}$ and are in general given by a symmetric 6×6 friction tensor $\eta_{i\alpha j\beta}(\mathbf{R})$, which consists of 21 independent elements each depending on six nuclear coordinates. These coordinates can be Cartesian $\mathbf{R} = (\mathbf{R}_1, \mathbf{R}_2)$ or expressed in the center-of-mass-centered spherical coordinate system $\mathbf{R} = (X, Y, Zd, \theta, \phi)$, which is commonly used for diatomics and described by Fig. 4.1 A.

4.2.2 Orbital-Dependent Friction and Density Functional Theory

Within ODF these 21 friction coefficients are obtained according to a Fermi-golden-rule-like expression resulting from time-dependent perturbation theory, which can be written in the quasi-static limit as [11, 25, 27, 36]

$$\eta^{\mathrm{ODF}}_{i\alpha j\beta}(\mathbf{R}) = 2\pi\hbar \sum_{\mathbf{k}ab} g^{i\alpha}_{\mathbf{k}ab}(\mathbf{R})^* \cdot g^{j\beta}_{\mathbf{k}ab}(\mathbf{R})\, \delta(\epsilon_{\mathbf{k}a} - \epsilon_{\mathrm{F}})\delta(\epsilon_{\mathbf{k}b} - \epsilon_{\mathrm{F}})\,. \tag{4.2}$$

The electron phonon matrix elements $g^{i\alpha}_{\mathbf{k}ab}$ describe the non-adiabatic coupling between two electronic states of the molecule at the metal surface with band indices a and b at wave vector $\mathbf{k}$, due to the motion of (adsorbate) atom i along direction α. In general, the ODF tensor can have different diagonal elements even for the same atom. This anisotropy yields very different friction forces when the atoms move (with the same velocity) in different directions. Its generally non-zero off-diagonal elements are responsible for coupling the motion in different directions and between both atoms in a way that is not accounted for by the PES. In particular, this can lead to a strong damping of the molecular stretch vibration of a diatomic molecule and thus a pronounced molecular anisotropy [20, 21, 23].

4.2.3 Neural Network Interpolation

In order to use the so-calculated $\eta^{\mathrm{ODF}}_{i\alpha j\beta}(\mathbf{R})$ in MDEF trajectory calculations of generic experimentally measurable observables, a continuous representation of this 6×6 tensor is required that can be evaluated at low computational cost. We have designed such a representation based on a symmetry-adapted neural network fit that is described briefly in Sec. 4.B and extensively in Chap. 6.

4.2.4 Local Density Friction Approximation

Within LDFA friction coefficients for hydrogen atoms $\eta^{\mathrm{H}}(\rho)$ are obtained from a spherical atom-in-jellium model with background density ρ, which is solved via density functional theory at the level of the local density [37] or generalized gradient approximation [38]. Mapping of the actual surface problem is accomplished by taking the electron density of the bare surface (without the molecule) at each atom's position $\rho(\mathbf{R}_i)$ as background density of the jellium [13]. This independent-atom approximation (IAA) results in electronic friction coefficients that are isotropic for each atom and depend on its own three coordinates alone. In Cartesian coordinates only diagonal elements of the friction tensor are non-zero,

$$\eta^{\mathrm{LDFA}}_{i\alpha j\beta}(\mathbf{R}) = \eta^{\mathrm{H}}(\rho(\mathbf{R}_i))\delta_{\alpha\beta}\delta_{ij} \tag{4.3}$$

A continuous representation of $\eta_{i\alpha j\beta}^{\mathrm{LDFA}}(\mathbf{R})$ for extensive MDEF trajectory calculations can be easily constructed [13, 39].

4.2.5 Isotropicalized Electronic Friction Tensor

Going beyond the IAA within LDFA is possible for example by determining the background electron density using an atoms-in-molecules technique (LDFA-AIM) [26]. However, this approach does not lift the isotropy, and as detailed in Sec. 4.A, cannot be applied to H_2 and D_2 molecules. The other way round, isotropic friction can be constructed from ODF, by neglecting the coupling between different directions and atoms plus averaging the remaining (generally anisotropic) friction over different directions

$$\eta_{i\alpha j\beta}^{\mathrm{ODF-iso}}(\mathbf{R}) = \frac{1}{3}\sum\nolimits_{\gamma} \eta_{i\gamma j\gamma}^{\mathrm{ODF}}(\mathbf{R})\delta_{ij}\delta_{\alpha\beta}\,. \tag{4.4}$$

This ODF-iso allows disentangling the influence of anisotropy from the very different electronic structure inherent to ODF and LDFA.

4

4.3 Results

4.3.1 Friction Coefficients

Fig. 4.2 A-C shows η_{Zd}, η_{dd} and η_{ZZ}, respectively, as obtained from equations 4.2-4.4 along the minimum energy reaction path for dissociative chemisorption over the bridge site as depicted in Fig. 4.2 D and Fig. 4.1 B. In particular the focus here is on these three particular friction coefficients, in order to compare with the earlier two-dimensional ODF calculations [21, 23]. The agreement is quite good except for some differences close to the transition state for η_{ZZ}^{ODF}. As the molecule approaches the surface, each model yields increasing friction for the six diagonal elements of the friction tensor, and the absolute values of the off-diagonal elements increase likewise in case of ODF. Furthermore, ODF directly reflects the strong rearrangement of (Kohn-Sham) orbitals when approaching the dissociation barrier by significantly higher friction along the molecular bond (and thus reaction) coordinate, resulting in $\eta_{dd}^{\mathrm{ODF}} \approx 3\eta_{dd}^{\mathrm{LDFA}}$ at

the transition state – in agreement with earlier work [21]. For the observables calculated below, friction beyond the dissociation barrier is not relevant. Quite remarkably, $\eta_{dd}^{\mathrm{ODF-iso}}$ ($\eta_{ZZ}^{\mathrm{ODF-iso}}$) and $\eta_{dd}^{\mathrm{LDFA}}$ ($\eta_{ZZ}^{\mathrm{LDFA}}$) are almost identical up to the transition state – and thus much more alike than what has originally been found for the diffusion of H atoms on Pd(100) [18, 40].

4.3.2 Dynamics

In order to study the effect of the different friction models on actual experimental observables, MDEF calculations are performed according to the quasi-classical trajectory method [29]. In view of the short interaction time of the molecules with the Cu(111) surface during all simulated trajectories, the fluctuating forces in Equation 4.1 are neglected.

4.3.3 Dissociative Chemisorption Probability

Fig. 4.3 shows the results for the dissociative chemisorption probability S_0 for both H_2 and D_2 molecular beams based on the SRP48-PES. Due to the construction of the latter [33, 34], already the adiabatic calculations yield good agreement with the experimental data [41, 42]. Inclusion of electronic friction reduces S_0, leading to even better agreement with the experimental data, in particular at high incidence energies. The reduction is strongest for ODF and weaker for LDFA and ODF-iso, which are very similar to each other. It can be rationalized by the differences of the friction models for the friction η_{dd} along reaction coordinate close to the dissociation barrier (see Fig. 4.2 B). This effect of η_{dd}^{ODF} on S_0 for H_2 and D_2 on Cu(111) has not been reported for two-dimensional ODF calculations [23]. Consequently, a high-dimensional treatment of ODF in MDEF, on an equal footing with LDFA [22], is important. However, the overall small effect of electronic friction on S_0 makes this not an optimal observable for experimental validation of the different friction models.

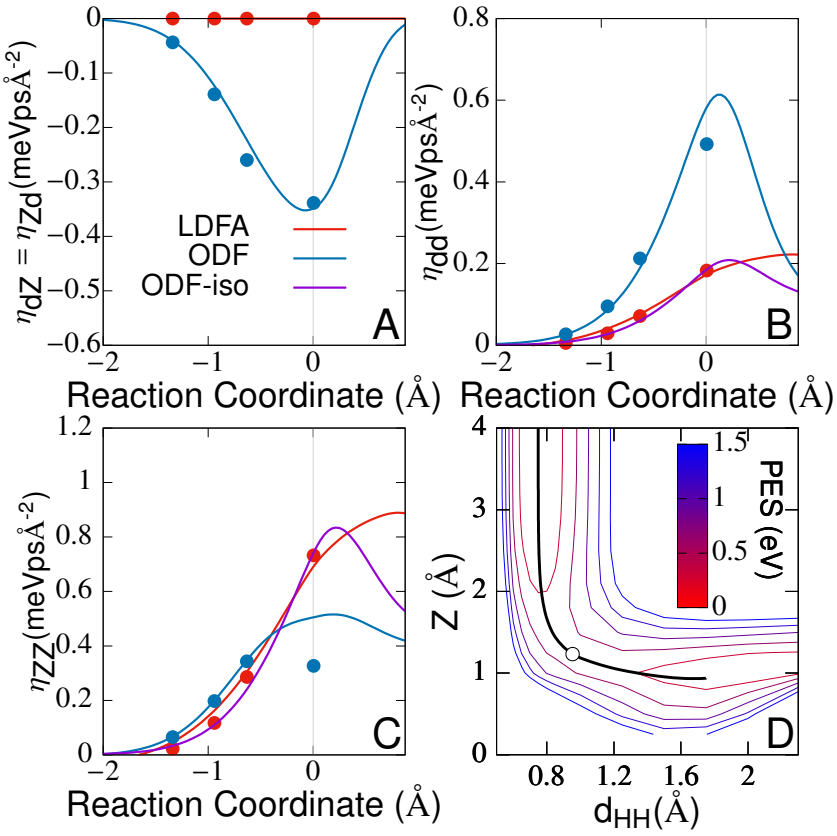

Figure 4.2: A-C show η_{dZ}, η_{dd} and η_{ZZ} in the molecular coordinate system (see Fig. 4.1 A), respectively, along the minimum energy reaction path for dissociative chemisorption over the bridge site (see Fig. 4.1 B) as depicted in D together with the corresponding two-dimensional PES cut. The blue, red and purple lines indicate the continuous representation from this chapter for ODF, LDFA and ODF-iso, respectively, as obtained from equations 4.2-4.4. Blue (red) dots show the ODF (LDFA) results from previous work of Luntz *et al.* [21, 23], and the reaction coordinate is defined in the same way as in that work. The barrier and thus the transition state for dissociation is located at the vertical gray line in A-C (0 Å) and indicated by the empty circle in D. Negative numbers up to transition state denote the approach from the gas-phase (i.e. decreasing heights Z above the surface).

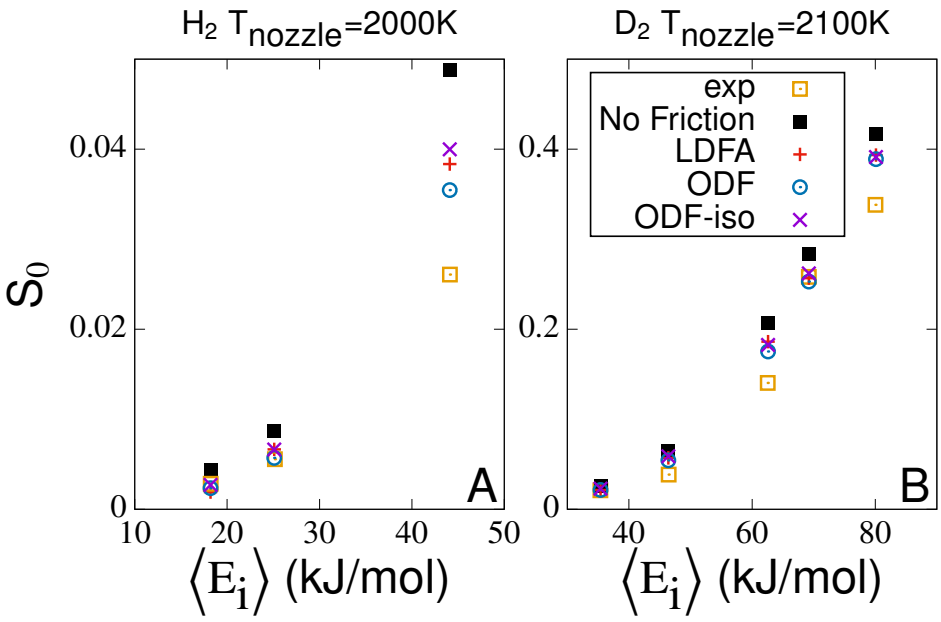

Figure 4.3: A(B) Calculated reaction probabilities S_0 based on the SRP48-PES for dissociative chemisorption of H_2 (D_2) molecular beams as a function of average normal incidence energy $\langle E_i \rangle$ for the indicated nozzle temperatures T_{nozzle} in comparison to experimental data (brown unfilled squares) from Ref. [41] (Ref. [42]). The calculations are adiabatic (filled black squares) or employ the LDFA (red plusses), ODF (blue circles) and ODF-iso (purple crosses) model for the electronic friction coefficients.

4.3.4 Vibrational De-Excitation

In contrast to the dissociative chemisorption probabilities, the vibrational de-excitation probabilities $P_{\mathrm{transition}}$ clearly yield a distinguishable difference between LDFA and ODF. $P_{\mathrm{transition}}$ is calculated as functions of incidence energy E_{i} from the scattered trajectories by a conventional binning procedure based on 50000 MDEF trajectories.. The concomitant average gain in translational energy $\langle \Delta E_{\mathrm{trans}} \rangle$ is calculated from the final center-of-mass velocities. As detailed in the supporting information, the error bars reflect the error due to statistical sampling of the initial conditions. Only by employing the newly developped continuous representation to compute a large amount of trajectories was it possible to reduce these errors so that the different electronic friction models can be distinguished. The discussion henceforth is focussed on de-excitation from vibrational state $\nu = 2, J = 1(2)$ to $\nu = 1, J = 1(2)$ for H_2 (D_2), respectively, as shown in Fig. 4.4. Unlike for other vibrational transitions [43], for this transition the results are not only qualitatively but even almost quantitatively identical to corresponding results obtained with the PW91-PES (see Sec. 4.D).

At low incidence energies, with increasing E_{i} more and more molecules come close enough to the surface so that the curvature of the PES and electronic friction lead to an increase of $P_{\mathrm{transition}}$. Both effects are additive and result in de-excitation probabilities that are up to 6(2) times larger for H_2 (Fig. 4.4C) and up to 3(2) times larger for D_2 with ODF(LDFA), respectively (Fig. 4.4D). At high incidence energies, the dissociation channel (see Fig. 4.3) becomes more effective, which is why $P_{\mathrm{transition}}$ decreases again in all cases. For the adiabatic simulations on the static surface, $\langle \Delta E_{\mathrm{trans}} \rangle$ is equal to the rovibrational energy loss of one vibrational quantum and thus by about $\sqrt{(}2)$ larger for H_2 than for D_2(Fig. 4.4A and B). Electronic friction reduces the energy gain. The reduction is almost twice as large for ODF compared to LDFA. The fact that it does not not very strongly depend on E_{i} for the energy range considered here suggests that it is dominated by η_{dd} and thus directly reflects the differences observed along the minimum energy path depicted in Fig. 4.2. Consequently, when comparing MDEF with other non-adiabatic models [44–46] for vibrational de-excitation, the new MDEF results suggest that it is crucial to also take into account whether the friction

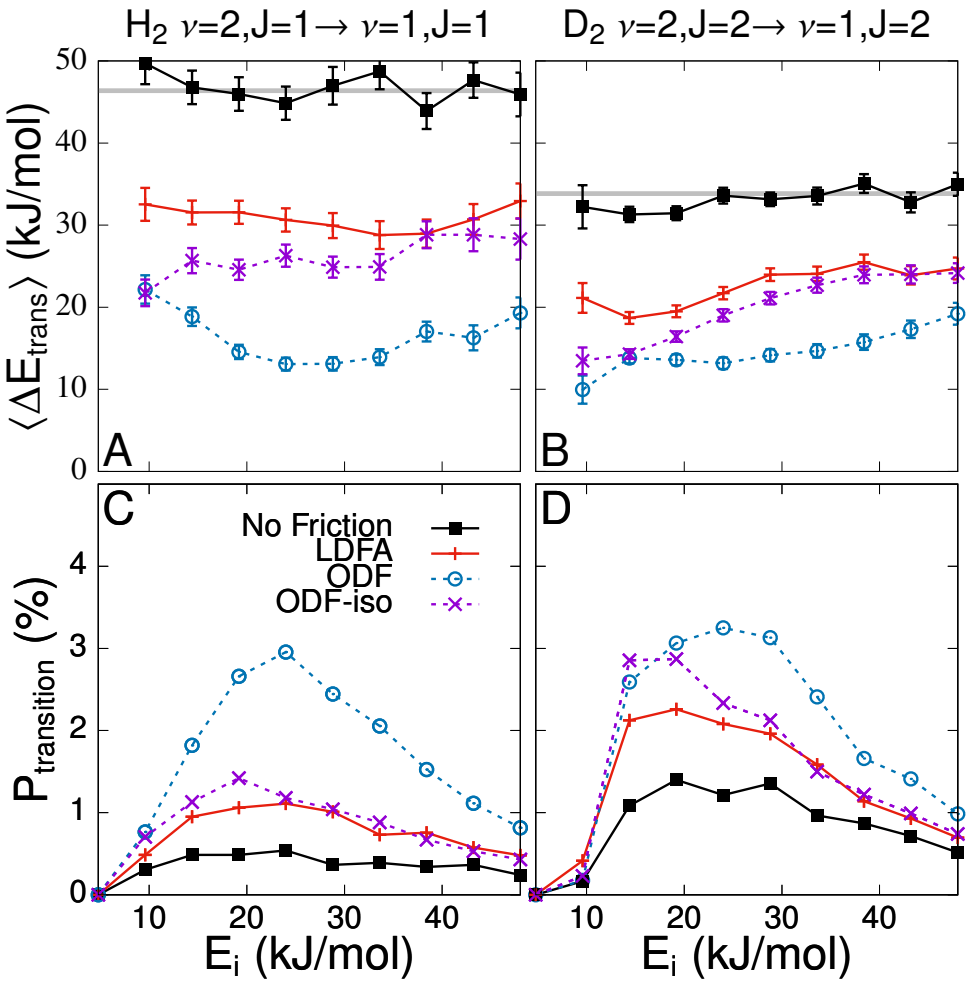

Figure 4.4: Vibrational de-excitation probabilities $P_{\text{transition}}$ (lower row) and concomitant average gain in translational energy $\langle \Delta E_{\text{trans}} \rangle$ (upper row) as a function of normal incidence energy E_{i} for state-to-state scattering using the SRP48-PES. Panels A,C (B,D) are for the transition from the rovibrational state $\nu = 2, J = 1(2)$ to $\nu = 1, J = 1(2)$ for H_2 (D_2). Shown are results from adiabatic calculations (filled black squares), as well as those including electronic friction according to the LDFA (red plusses), ODF (blue circles) or ODF-iso (purple crosses) models. The error bars indicate the error due to statistical sampling as described in detail in Sec. 4.C.

coefficients include any molecular anisotropy. Unfortunately, since molecular beam experiments for this system have hitherto focused on rovibrational excitation rather than de-excitation [47–49], experimental verification of this effect is still pending.

Although ODF-iso inherits the spurious memory effects as well as going beyond the independent atom approximation from ODF, quite remarkably, for $E_\mathrm{i} > 15(20)$ kJ/mol for H_2 (D_2), results obtained with ODF-iso are almost identical to LDFA. That means that (at least in this energy range) these do not affect the dynamics and the molecular anisotropy is the most important difference. [50] If this can be experimentally validated, it would greatly encourage future theoretical work to develop extensions to LDFA that can account for this anisotropy.

4.4 Conclusions & Outlook

In summary, I have obtained different observables for H_2 and D_2 on Cu(111) from extensive MDEF trajectory calculations for the first time using full-dimensional friction tensors based on both LDFA *and* ODF. The molecular anisotropy as described by ODF and absent from LDFA leads to strongly enhanced friction for motion along the molecular axis when the molecules are close to the surface. The dissociative sticking probability is almost negligibly reduced compared to adiabatic simulations. The effect is slightly stronger for ODF compared to LDFA and improves the agreement with experimental data in both cases. For the state-to-state scattering of vibrationally excited molecules (from $\nu = 2, J = 1(2)$ to $\nu = 1, J = 1(2)$ for H_2 (D_2)), the newly developed MDEF model predicts up to six (two) times larger vibrational de-excitation probabilities with ODF (LDFA) compared to adiabatic simulations. Remarkably, isotropicalization of ODF yields results almost identical to LDFA for incidence energies larger than 15(20) kJ/mol for H_2 (D_2). The predicted differences between the vibrational de-excitation probabilities are a “fingerprint” of the molecular anisotropy as described by ODF. Recently suggested techniques to prepare H_2 molecular beams with $1 \leq \nu \leq 4$ [51] should allow testing for this “fingerprint”. This would provide unprecedented insights into the accuracy of state-of-the-art electronic friction models for molecules and

allow analyzing the importance of concomitant approximations.

4.5 Computational Details

The electron phonon matrix elements $g^{i\alpha}_{\mathbf{k}ab} = \langle\phi_{\mathbf{k}\mathrm{a}}|\frac{\partial v_{\mathrm{KS}}}{\partial \mathbf{R}_{i\alpha}}|\phi_{\mathbf{k}\mathrm{b}}\rangle$ in Equation 4.2 are obtained from the change of Kohn-Sham potential $\frac{\partial v_{\mathrm{KS}}}{\partial \mathbf{R}_{i\alpha}}$ with respect to nuclear coordinate $\mathbf{R}_{i\alpha}$, which is obtained from density functional perturbation theory (DFPT) [52] employing the PW91 [53] exchange-correlation functional as implemented in the Quantum Espresso package[54]. Surfaces are modeled by 2×2 Cu(111) slabs with 4 layers and 10 Å of vacuum. A planewave cut-off energy of 816 eV is used, together with ONCV pseudopotentials [55] from the SG15 [56] library and an 18x18 **k**-point grid. These settings reproduce the PW91-PES from Ref. [35] up to a few meV. They also enable an accurate evaluation of the sum over electronic states in Equation 4.2 at the Fermi level using an equivalent Gaussian envelope technique to broaden the δ-function with a width of 0.6 eV as suggested in Ref. [27]. It should be noted here that this implies the possible presence of spurious electronic memory effects as argued in Ref. [28] and that care should be taken as this broadening can be system specific.

The neural network fits for the 21 independent elements of $\eta^{\mathrm{ODF}}_{i\alpha j\beta}(\mathbf{R})$ are based on $\approx$ 30000 ODF coefficients obtained from DFT calculations on the same 7 lateral sites that have been used to construct the SRP48-PES [34]. LDFA coefficients are obtained by extracting the background electron density $\rho(\mathbf{R}_i)$ from a DFT calculation with same the computational setup as described above. Employing the functional form for $\eta^{\mathrm{H}}(\rho)$ suggested in Ref. [39] a grid (in $\mathbf{R}_i$) of friction coefficients is obtained and used to construct a three-dimensional neural network interpolations for $\eta^{\mathrm{H}}(\rho(\mathbf{R}_i))$ based on the symmetry-adapted coordinates [57, 58] in order to obtain a continuous representation of $\eta^{\mathrm{LDFA}}_{i\alpha j\beta}(\mathbf{R})$.

4.A LDFA "Atoms in Molecules" for H_2 and D_2

Rittmeyer *et al.* have suggested an extension of the local density friction approximation (LDFA) going beyond the independent atom approximation [26], accounting for molecular properties by means of the atoms-in-molecules (AIM) technique according to Hirshfeld [59]. The authors have used this LDFA-AIM scheme very successfully to model the non-adiabatic vibrational damping of CO adsorbed on Cu(100) and Pt(111). However, this scheme cannot be applied to the adsorption or scattering dynamics of H_2 or D_2 on any metal surface, because it yields unrealistic non-zero friction coefficients for these two molecules in the gas phase as illustrated in Fig. 4.5 (an extension of Fig. 4.2).

This can be understood by having a closer look at how the embedding density $\rho^{\mathrm{AIM}}_{\mathrm{emb},i}$ for an atom at positions $\mathbf{R}_i$ (i.e. background density for the atoms-in-jellium model underlying the LDFA [13]) is constructed [26]:

$$\rho^{\mathrm{AIM}}_{\mathrm{emb},i} = \left[1 - w_i^{\mathrm{Hirshfeld}}(\mathbf{R}_i)\right] \cdot \rho^{\mathrm{SCF}}(\mathbf{R}_i) \; . \tag{4.5}$$

Here ρ^{SCF} is the self-consistent density from the DFT calculation of the surface including the molecule. The Hirshfeld weight is defined based on electron densities of N isolated atoms ρ_i^{atom} at the same positions $\mathbf{R}_i$ [59]

$$w_i^{\mathrm{Hirshfeld}}(\mathbf{R}_i) = \frac{\rho_i^{\mathrm{atom}}(\mathbf{R}_i)}{\sum_{j=1}^{N} \rho_j^{\mathrm{atom}}(\mathbf{R}_i)} \; . \tag{4.6}$$

Since the density rearrangement in a H_2 (or equivalently D_2) molecule in the gas phase hardly affects the electron density at the nucleus, the superposition of electron densities of two non-interacting H (or equivalently D) atoms

$$\rho^{\mathrm{SCF}}(\mathbf{R}_i) \approx \rho_1^{\mathrm{H-atom}}(\mathbf{R}_i) + \rho_2^{\mathrm{H-atom}}(\mathbf{R}_i) \tag{4.7}$$

is a good approximation. Equation 4.6 then simplifies to

$$\rho^{\mathrm{AIM}}_{\mathrm{emb},1(2)} \approx \rho_{2(1)}^{\mathrm{H-atom}}(\mathbf{R}_{1(2)}) = \rho^{\mathrm{H-atom}}(d_{\mathrm{H-H}}). \tag{4.8}$$

Fig. 4.6 shows that this density is still quite seizable and the corresponding H-atom-in-jellium model with this background density results in a significant friction coefficient

$\eta^{\mathrm{H}}(\rho^{\mathrm{H-atom}}(d_{\mathrm{H-H}}))$. Transformation into the molecular coordinate system then yields approximately half of this value for $\eta_{dd}^{\mathrm{LDFA-AIM}}$ (twice for $\eta_{ZZ}^{\mathrm{LDFA-AIM}}$) in the gas phase as denoted by the reaction coordinate value -2 in Fig. 4.5B(C), respectively.

We emphasize that H_2 and D_2 are exceptional due to their short bond lengths. According to testing procedure explained in the previous paragraph, LDFA-AIM should still be applicable to other homo-nuclear diatomics.

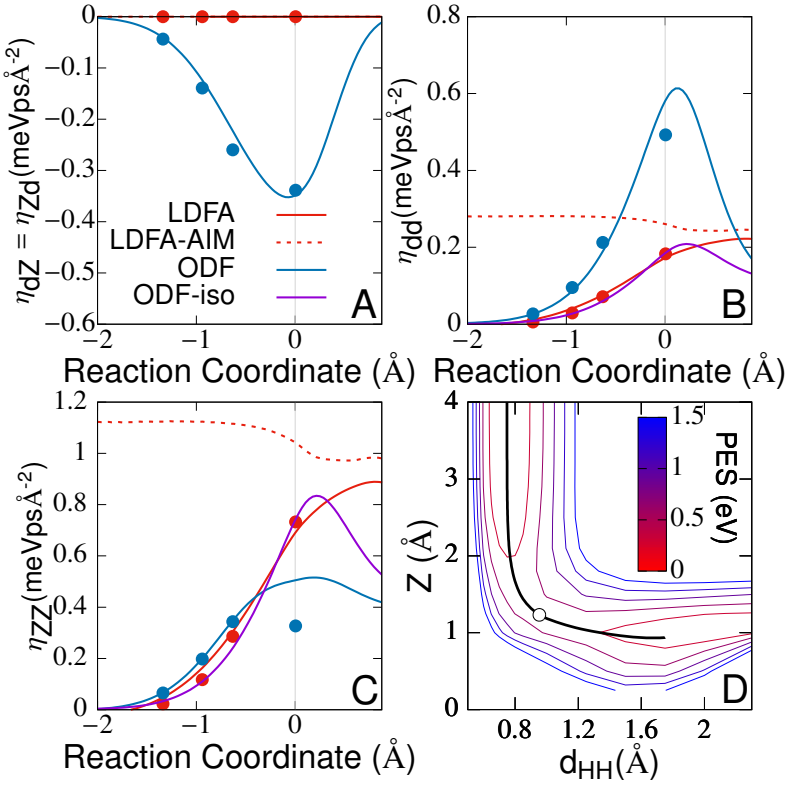

Figure 4.5: Same as Fig. 4.2, but additionally includes friction coefficients as resulting from the LDFA-AIM scheme [26] (dashed red line). Note that $\eta_{dZ}^{\mathrm{LDFA-AIM}} = 0$ since LDFA-AIM yields isotropic friction like LDFA relying on the independent atom approximation.[13]

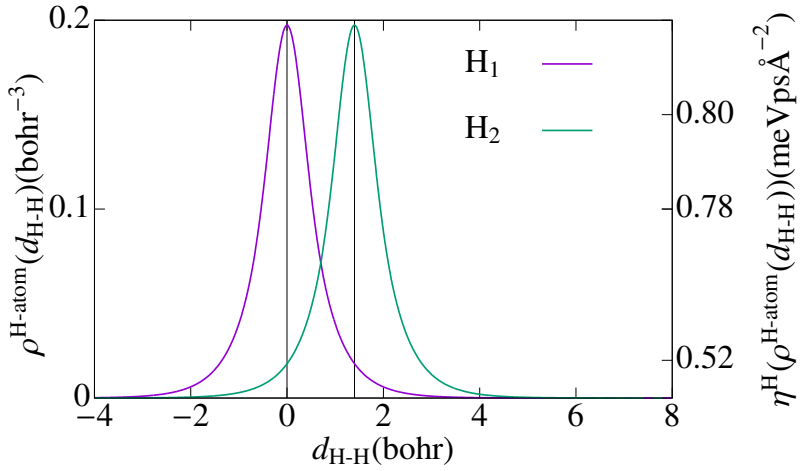

Figure 4.6: One-dimensional cut through electron densities of non-interacting hydrogen atoms $\rho^{\text{H}-\text{atom}}$ located at the origin (purple curve) and at the experimental bond distance $d_{\text{H}-\text{H}} \approx 1.4$ bohr (green curve). $\rho^{\text{H}-\text{atom}}$ has been obtained from a DFT calculation with the PW91 exchange correlation functional [53], i.e. using the same computational setup as the other DFT calculations in this chapter. The second y-axis shows the electronic friction coefficient $\eta^{\text{H}}(\rho^{\text{H}-\text{atom}}(d_{\text{H}-\text{H}}))$ as calculated based on the corresponding H-atom-in-jellium model for the background electron density $\rho^{\text{H}-\text{atom}}(d_{\text{H}-\text{H}})$.

4.B Continuous Representation of 6×6 Friction Tensors

4.B.1 Symmetry-Adapted Neural Network Representation

In principal, computationally efficient neural-network-based techniques as developed for potential energy surfaces in gas-surface dynamics can be adapted [57, 58, 60–62] – promising to accurately describe the 21 different elements of the symmetric 6×6 friction tensor as functions of the six molecular degrees of freedom, thus avoiding low-dimensional analytic forms [23, 44]. However, these 21 tensor elements are intertwined by symmetry of the static surface. This is not accounted for by the aforementioned techniques. To ensure that the friction tensor also represents the correct combination of translational and orientational symmetry and can account for molecular anisotropy, a molecular coordinate system is first introduced that denotes the center of mass positions (X, Y, Z), bond length d and spherical orientation (θ, ϕ), as depicted in Fig. 4.1A. For every molecular configuration a transformation $T(\theta, \phi)$ that transforms to the reference orientation $\theta_0 = \phi_0 = 90°$ is constructed, which characterizes the majority of dissociation paths with the lowest barriers [35]. The 6D electronic friction tensor is then defines as

$$\eta^{\mathrm{ODF}}(\mathbf{R}) \approx T(\theta, \phi)\, \tilde{\eta}^{\mathrm{ODF}}(X, Y, Z, d)\, T^{-1}(\theta, \phi) \tag{4.9}$$

because the 21 independent friction coefficients $\tilde{\eta}^{\mathrm{ODF}}_{i\alpha j\beta}(X, Y, Z, d)$ can now be fitted with 21 independent neural networks using the symmetry-adapted coordinates for fcc(111) surfaces as described by Meyer *et al.* [57, 58]. Sec. 4.B.2 provides a verification that $\tilde{\eta}^{\mathrm{ODF}}$ is rather independent of the choice of the reference orientation and the fitting accuracy of the neural network is discussed in Sec. 4.B.3.

4.B.2 Choice of Reference Angles ϕ_0 and θ_0

Fig. 4.7 shows the influence of the reference angle ϕ_0 and θ_0 as defined in the context of Eq. 4.9 on ODF coefficients obtained from DFT calculations. η_{dZ}, η_{dd} and η_{ZZ} do not depend significantly on the choice of ϕ_0, whereas θ_0 has a slightly bigger effect. However, since $\theta_0 = \phi_0 = 90°$ characterizes the majority of dissociation paths with

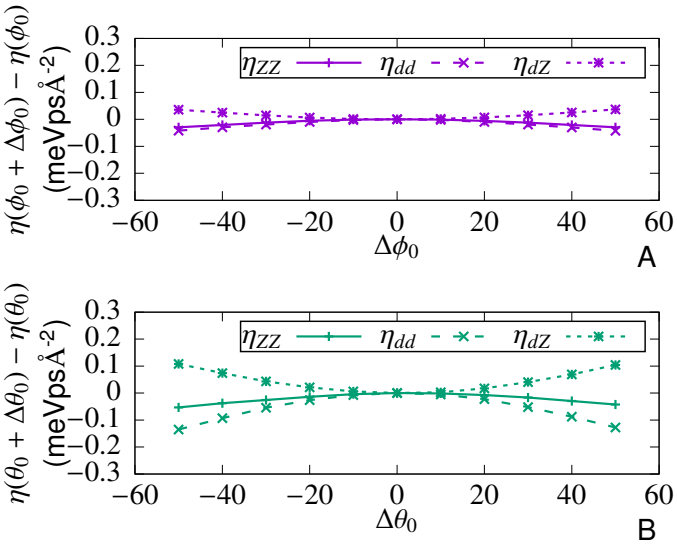

Figure 4.7: A (B) shows the influence of the reference angle ϕ_0 (θ_0) as defined in the context of Eq. 4.9 on ODF coefficients obtained from DFT calculations. The molecule is located at the transition state over the bridge site. Solid, long-dashed and short-dashed lines indicate η_{dZ}, η_{dd} and η_{ZZ}, respectively.

the lowest barriers [35] and due to the overall small effects of electronic friction on the dynamics, I am confident that these effects are not significant. Future work on other systems might require to explicitly include the angular orientation in the neural network fits.

4.B.3 Fitting Accuracy

This section details the fitting quality for the neural networks used to obtain continuous representations of the friction coefficients for the MDEF trajectory calculations. Since a very accurate such representation can be easily obtained for the local density friction approximation (LDFA) [39], only details for orbital-dependent friction (ODF) scheme are reported here.

Fig. 4.8 shows the root-mean-square errors (RMSEs) of the neural network (NN)

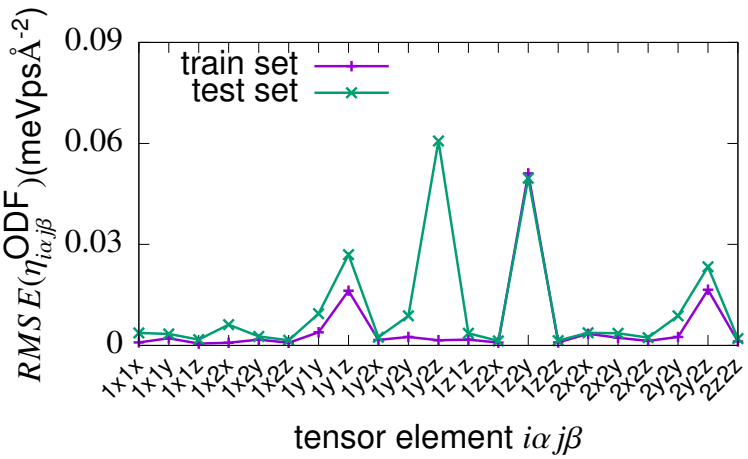

Figure 4.8: Root-mean-square errors (RMSEs) of the neural network fits for each of the 21 different elements $i\alpha j\beta$ of the symmetric 6×6 orbital-dependent friction (ODF) tensor $\eta^{\mathrm{ODF}}_{i\alpha j\beta}$. $i,j\in\{1,2\}$ indicate the two hydrogen atoms and $\alpha,\beta\in\{x,y,z\}$ denote Cartesian coordinates.

fits for each of the 21 different elements of the symmetric 6×6 ODF tensor $\eta^{\mathrm{ODF}}_{i\alpha j\beta}$, where $i,j\in\{1,2\}$ indicate the two hydrogen atoms and $\alpha,\beta\in\{x,y,z\}$ denote Cartesian coordinates. These fits are based on $\approx$ 30000 data points obtained from DFT calculations on the same 7 lateral sites that have been used to construct the SRP48-PES [34]. The training sets for the NN fits also contain some configurations of H_2 and D_2 at distances from the surfaces larger than 4 Å. At these distances, both the PW91-[35] and SRP48-PES[34] yield negligible molecule-surface interaction and hence, consistently, also the corresponding ODF coefficients are essentially zero. Since this "gas-phase region" is easily fitted by the NNs, those configurations are not included in the error analysis in order to avoid a bias of the RMSE.

The RMSEs are largest for the NN fits for the off-diagonal elements that describe the coupling between the z and y directions, both for the the same ($1y1z$, $2y2z$) and even more for different ($1y2z$, $1z2y$) hydrogen atoms. Using very similar convergence criteria in the DFT calculations for electron phonon matrix elements as well as for the Gaussian broadening of the δ-function for the sum over states, a very similar

convergence of the ODF coefficients of ±10 % as reported by Maurer *et al.* in Refs [20, 27] is expected. This systematic error in the input data that forms the training and test sets for our NN fits is comparable to the aforementioned worst RMSEs, while the fits for all other 17 different tensor elements are up to an order of magnitude more accurate. Consequently, the fitting accuracy achieved here is considered more than sufficient for the present study.

A representative overview of the accuracy of the fits in this chapter is given in Fig. 4.9 by comparing their values for η_{dZ}, η_{dd} and η_{ZZ} along the minimum energy reaction path for dissociative chemisorption over the bridge site as obtained directly from our DFT calculations. These calculations were done separately on a dense grid of points along the reaction path and not included in the NN fits. For all of these three elements of the friction tensor, which are most important for the MDEF trajectory calculations presented, the agreement is excellent.

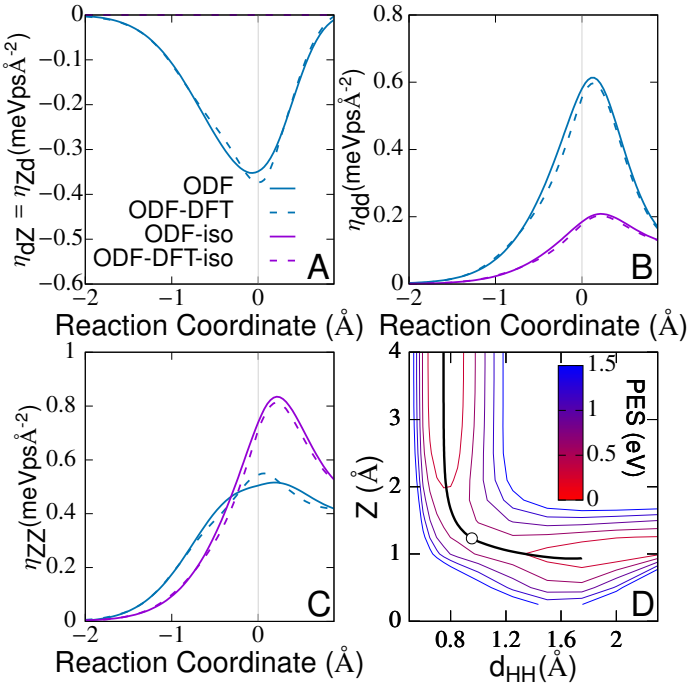

Figure 4.9: Similar to Fig. 4.2. A-C show η_{dZ}, η_{dd} and η_{ZZ} in the molecular coordinate system, respectively, along the minimum energy reaction path for dissociative chemisorption over the bridge site as depicted in D together with the corresponding two-dimensional PES cut. See Fig. 4.1 for the coordinate system. Blue (purple) show tensor elements for the ODF (ODF-iso) scheme. Dashed lines are for values obtained directly from our DFT calculations on a dense grid of points along the reaction path and not included in the NN fits. Solid lines are from the NN fits evaluated on the same grid.

4.C Errors Due to Statistical Sampling

In this section the errors of the quantities shown in Fig. 4.4 are discussed. These errors arise from the statistical sampling of the initial conditions (angular orientation of the molecule, lateral impact site, bond distance and corresponding velocity according to the classical equivalent of the vibrational state) with a finite number of molecular dynamics trajectories N [30, 35].

4.C.1 Inelastic Scattering Probabilities $P_{\text{transition}}$

The standard error of the state-to-state-specific inelastic scattering probabilities $P_{\text{transition}}$ shown in Figures 4 C and D are given by

$$\sigma^{\text{SE}}_{P_{\text{transition}}}(N) = \sqrt{\frac{P_{\text{transition}}\,(1 - P_{\text{transition}})}{N}}. \tag{4.10}$$

Since $\sigma^{\text{SE}}_{P_{\text{transition}}}(N) \leq \frac{0.5}{\sqrt{N}}$, the errors of $P_{\text{transition}}$ due to statistical sampling are completely negligible on the scale of the plots for the large amount of trajectories simulated here ($N = 50000$). Consequently, no error bars have been included. The same argument holds for the dissociative sticking probabilities S_0 shown in Fig. 4.2 as well.

4.C.2 Average Translational Energy Gain $\langle \Delta E_{\text{trans}} \rangle$

Concerning the average translational energy gain $\langle \Delta E_{\text{trans}} \rangle$ for vibrationally inelastic scattering from vibrational state $\nu = 2, J = 1(2)$ to $\nu = 1, J = 1(2)$ for H_2 (D_2) presented in Figures 4 A and B, the standard deviation

$$\sigma_{\langle \Delta E_{\text{trans}} \rangle} = \sqrt{\frac{1}{N_{\text{scatt}}} \sum_{i}^{N_{\text{scatt}}} \left(\Delta E^i_{\text{trans}} - \langle \Delta E_{\text{trans}} \rangle \right)^2} \quad . \tag{4.11}$$

is calculated first. $\Delta E^i_{\text{trans}}$ is the change in translational energy corresponding to scattered trajectory i. N_{scatt} denotes the amount of scattered trajectories that undergo the specific aforementioned transition, i.e.

$$N_{\text{scatt}} \;=\; P_{\text{transition}} \cdot N \quad . \tag{4.12}$$

For the results in this chapter the standard deviation is considered to be an estimator for the error of a single trajectory i, indicating the spread of $\Delta E^i_{\mathrm{trans}}$ around the average $\langle \Delta E_{\mathrm{trans}} \rangle$. Then, according to the "law of large numbers", the standard error

$$\sigma^{\mathrm{SE}}_{\langle \Delta E_{\mathrm{trans}} \rangle} = \frac{\sigma_{\langle \Delta E_{\mathrm{trans}} \rangle}}{\sqrt{N_{\mathrm{scatt}}}} = \frac{1}{N_{\mathrm{scatt}}} \sqrt{\sum_{i}^{N_{\mathrm{scatt}}} \left(\Delta E^i_{\mathrm{trans}} - \langle \Delta E_{\mathrm{trans}} \rangle \right)^2} \tag{4.13}$$

is an estimator for the error of $\langle \Delta E_{\mathrm{trans}} \rangle$ with respect to the statistical sampling. Assuming a 95% confidence interval for a normal distribution, the error bars in Figures 4 A and B are obtained from $1.96 \cdot \sigma^{\mathrm{SE}}_{\langle \Delta E_{\mathrm{trans}} \rangle}$. Since the corresponding scattering probabilities $P_{\mathrm{transition}}$ can be less than 1 % (see Figures 4 C and D), at least 10^4 trajectories are required for those errors to become sufficiently small so that the predictions of the different electronic friction models are clearly distinguishable.

4.D Vibrational De-Excitation for PW91-PES

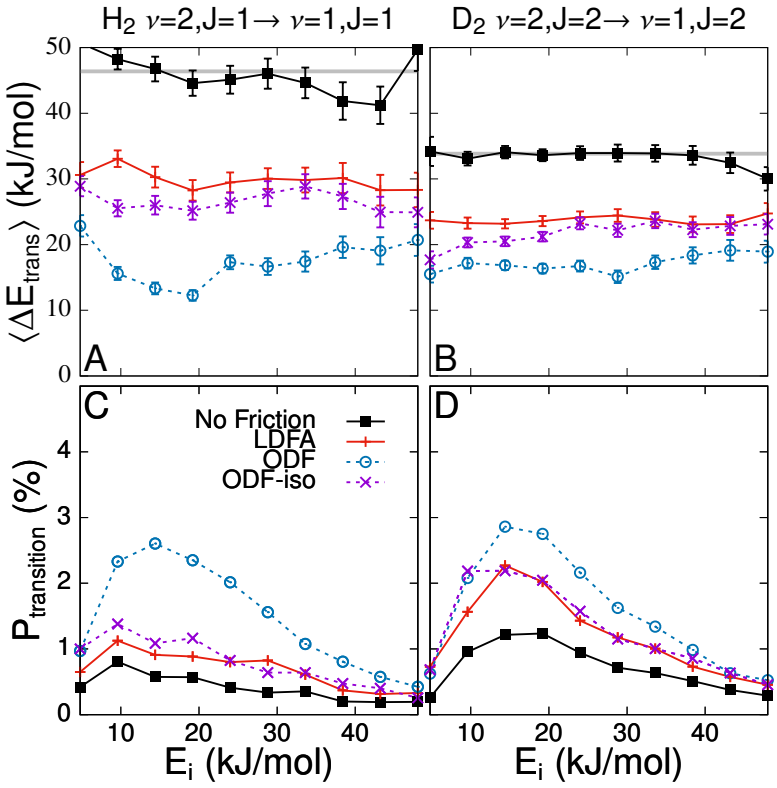

Figure 4.10: Same as Fig. 4.4, but trajectories calculated using a PW91 [35] instead of a SRP48 PES [34]. Vibrational de-excitation probabilities $P_{\text{transition}}$ (lower row) and concomitant average gain in translational energy $\langle \Delta E_{\text{trans}} \rangle$ (upper row) as a function of normal incidence energy E_{i} for state-to-state scattering. Panels A,C (B,D) are for the transition from the rovibrational state $\nu = 2, J = 1(2)$ to $\nu = 1, J = 1(2)$ for H_2 (D_2). Shown are results from adiabatic calculations (filled black squares), as well as those including electronic friction according to the LDFA (red plusses), ODF (blue circles) or ODF-iso (purple crosses) models. The error bars indicate the error due to statistical sampling as described in Section 4.C.

References

[1] P. Spiering and J. Meyer. "Testing Electronic Friction Models: Vibrational De-Excitation in Scattering of H_2 and D_2 from Cu(111)". In: *J. Phys. Chem. Lett.* 9 (2018), pp. 1803–1808. DOI: 10.1021/acs.jpclett.7b03182.

[2] A. M. Wodtke, J. C. Tully, and D. J. Auerbach. "Electronically Non-Adiabatic Interactions of Molecules at Metal Surfaces: Can We Trust the Born-Oppenheimer Approximation for Surface Chemistry?" In: *Int. Rev. Phys. Chem.* 23.4 (2004), pp. 513–539.

[3] G.-J. Kroes. "Frontiers in Surface Scattering Simulations". In: *Science* 321 (2008), pp. 794–797. DOI: 10.1126/science.1157717.

[4] K. Golibrzuch, N. Bartels, D. J. Auerbach, and A. M. Wodtke. "The Dynamics of Molecular Interactions and Chemical Reactions at Metal Surfaces: Testing the Foundations of Theory". In: *Annu. Rev. Phys. Chem.* 66 (2015), pp. 399–425. DOI: 10.1146/annurev-physchem-040214-121958.

[5] A. M. Wodtke. "Electronically Non-Adiabatic Influences in Surface Chemistry and Dynamics". In: *Chem. Soc. Rev.* 45 (2016), pp. 3641–3657. DOI: 10.1039/C6CS00078A.

[6] N. Shenvi, S. Roy, and J. C. Tully. "Nonadiabatic Dynamics at Metal Surfaces: Independent-Electron Surface Hopping". In: *J. Chem. Phys.* 130 (2009), p. 174107. DOI: 10.1063/1.3125436.

[7] J. Meyer and K. Reuter. "Electron–Hole Pairs during the Adsorption Dynamics of O_2 on Pd(100): Exciting or Not?" In: *New J. Phys.* 13 (2011), p. 085010. DOI: 10.1088/1367-2630/13/8/085010.

[8] I. G. Ryabinkin and A. F. Izmaylov. "Mixed Quantum-Classical Dynamics Using Collective Electronic Variables: A Better Alternative to Electronic Friction Theories". In: *J. Phys. Chem. Lett.* 8 (2017), pp. 440–444. DOI: 10.1021/acs.jpclett.6b02712.

[9] W. Dou, G. Miao, and J. E. Subotnik. "Born-Oppenheimer Dynamics, Electronic Friction, and the Inclusion of Electron-Electron Interactions". In: *Phys. Rev. Lett.* 119 (2017), p. 046001. DOI: 10.1103/PhysRevLett.119.046001.

[10] S. P. Rittmeyer, J. Meyer, and K. Reuter. "Nonadiabatic Vibrational Damping of Molecular Adsorbates: Insights into Electronic Friction and the Role of Electronic Coherence". In: *Phys. Rev. Lett.* 119 (2017), p. 176808. DOI: 10.1103/PhysRevLett.119.176808.

[11] M. Head-Gordon and J. C. Tully. "Molecular Dynamics with Electronic Frictions". In: *J Chem Phys* 103 (1995), pp. 10137–10145. DOI: 10.1063/1.469915.

[12] M. Alducin, R. Díez Muiño, and J. I. Juaristi. "Non-Adiabatic Effects in Elementary Reaction Processes at Metal Surfaces". In: *Prog. Surf. Sci.* 92 (2017), pp. 317–340. DOI: 10.1016/j.progsurf.2017.09.002.

[13] J. I. Juaristi, M. Alducin, R. D. Muiño, H. F. Busnengo, and A. Salin. "Role of Electron-Hole Pair Excitations in the Dissociative Adsorption of Diatomic Molecules on Metal Surfaces". In: *Phys. Rev. Lett.* 100 (2008), p. 116102. DOI: 10.1103/PhysRevLett.100.116102.

[14] D. Novko, M. Blanco-Rey, M. Alducin, and J. I. Juaristi. "Surface Electron Density Models for Accurate *Ab Initio* Molecular Dynamics with Electronic Friction". In: *Phys. Rev. B* 93 (2016), p. 245435. DOI: 10.1103/PhysRevB.93.245435.

[15] B. Hellsing and M. Persson. "Electronic Damping of Atomic and Molecular Vibrations at Metal Surfaces". In: *Phys Scr* 29 (1984), p. 360. DOI: 10.1088/0031-8949/29/4/014.

[16] S. M. Janke, D. J. Auerbach, A. M. Wodtke, and A. Kandratsenka. "An Accurate Full-Dimensional Potential Energy Surface for h(111): Importance of Nonadiabatic Electronic Excitation in Energy tTansfer and Adsorption". In: *J. Chem. Phys.* 143 (2015), p. 124708. DOI: 10.1063/1.4931669.

[17] O. Bünermann, H. Jiang, Y. Dorenkamp, A. Kandratsenka, S. M. Janke, et al. "Electron-Hole Pair Excitation Determines the Mechanism of Hydrogen Atom Adsorption". In: *Science* 350 (2015), pp. 1346–1349. DOI: 10.1126/science.aad4972.

[18] M. Askerka, R. J. Maurer, V. S. Batista, and J. C. Tully. "Role of Tensorial Electronic Friction in Energy Transfer at Metal Surfaces". In: *Phys. Rev. Lett.* 116 (2016), p. 217601. DOI: 10.1103/PhysRevLett.116.217601.

[19] K.-i. Inoue, K. Watanabe, T. Sugimoto, Y. Matsumoto, and T. Yasuike. "Disentangling Multidimensional Nonequilibrium Dynamics of Adsorbates: CO Desorption from Cu(100)". In: *Phys. Rev. Lett.* 117 (2016), p. 186101. DOI: 10.1103/PhysRevLett.117.186101.

[20] R. J. Maurer, B. Jiang, H. Guo, and J. C. Tully. "Mode Specific Electronic Friction in Dissociative Chemisorption on Metal Surfaces: H_2 on Ag(111)". In: *Phys. Rev. Lett.* 118 (2017), p. 256001. DOI: 10.1103/PhysRevLett.118.256001. arXiv: 1705.09753 [cond-mat.mtrl-sci].

[21] A. C. Luntz, I. Makkonen, M. Persson, S. Holloway, D. M. Bird, et al. "Comment on "Role of Electron-Hole Pair Excitations in the Dissociative Adsorption of Diatomic Molecules on Metal Surfaces"". In: *Phys. Rev. Lett.* 102 (2009), p. 109601. DOI: 10.1103/PhysRevLett.102.109601.

[22] J. I. Juaristi, M. Alducin, R. D. Muiño, H. F. Busnengo, and A. Salin. "Juaristi et al. Reply:" in: *Phys. Rev. Lett.* 102 (2009), p. 109602. DOI: 10.1103/PhysRevLett.102.109602.

[23] A. C. Luntz and M. Persson. "How Adiabatic Is Activated Adsorption/Associative Desorption?" In: *J. Chem. Phys.* 123 (2005), p. 074704. DOI: 10.1063/1.2000249.

[24] V. Krishna and J. C. Tully. "Vibrational Lifetimes of Molecular Adsorbates on Metal Surfaces". In: *J. Chem. Phys.* 125 (2006), p. 054706. DOI: 10.1063/1.2227383.

[25] M. Forsblom and M. Persson. "Vibrational Lifetimes of Cyanide and Carbon Monoxide on Noble and Transition Metal Surfaces". In: *J. Chem. Phys.* 127 (2007), p. 154303. DOI: 10.1063/1.2794744.

[26] S. P. Rittmeyer, J. Meyer, J. I. Juaristi, and K. Reuter. "Electronic Friction-Based Vibrational Lifetimes of Molecular Adsorbates: Beyond the Independent-Atom Approximation". In: *Phys. Rev. Lett.* 115 (2015), p. 046102. DOI: 10.1103/PhysRevLett.115.046102.

[27] R. J. Maurer, M. Askerka, V. S. Batista, and J. C. Tully. "Ab Initio Tensorial Electronic Friction for Molecules on Metal Surfaces: Nonadiabatic Vibrational Relaxation". In: *Phys. Rev. B* 94 (2016), p. 115432. DOI: 10.1103/PhysRevB.94.115432.

[28] D. Novko, M. Alducin, M. Blanco-Rey, and J. I. Juaristi. "Effects of Electronic Relaxation Processes on Vibrational Linewidths of Adsorbates on Surfaces: The Case of CO/Cu(100)". In: *Phys. Rev. B* 94 (2016). DOI: 10.1103/PhysRevB.94.224306.

[29] G.-J. Kroes, J. I. Juaristi, and M. Alducin. "Vibrational Excitation of H2 Scattering from Cu(111): Effects of Surface Temperature and of Allowing Energy Exchange with the Surface". In: *J. Phys. Chem. C* 121 (2017), pp. 13617–13633. DOI: 10.1021/acs.jpcc.7b01096.

[30] C. Díaz, E. Pijper, R. A. Olsen, H. F. Busnengo, D. J. Auerbach, et al. "Chemically Accurate Simulation of a Prototypical Surface Reaction: H2 Dissociation on Cu(111)". In: *Science* 326 (2009), pp. 832–834. DOI: 10.1126/science.1178722.

[31] F. Nattino, A. Genova, M. Guijt, A. S. Muzas, C. Díaz, et al. "Dissociation and Recombination of D_2 on Cu(111): Ab Initio Molecular Dynamics Calculations and Improved Analysis of Desorption Experiments". In: *J. Chem. Phys.* 141 (2014), p. 124705. DOI: 10.1063/1.4896058.

[32] G.-J. Kroes and C. Díaz. "Quantum and Classical Dynamics of Reactive Scattering of H2 from Metal Surfaces". In: *Chem. Soc. Rev.* 45 (2016), pp. 3658–3700. DOI: 10.1039/C5CS00336A.

[33] C. Díaz, R. A. Olsen, D. J. Auerbach, and G.-J. Kroes. "Six-Dimensional Dynamics Study of Reactive and Non Reactive Scattering of H2 from Cu(111) Using a Chemically Accurate Potential Energy Surface". In: *Phys. Chem. Chem. Phys.* 12 (2010), pp. 6499–6519. DOI: 10.1039/C001956A.

[34] A. Mondal, M. Wijzenbroek, M. Bonfanti, C. Díaz, and G.-J. Kroes. "Thermal Lattice Expansion Effect on Reactive Scattering of H2 from Cu(111) at Ts = 925 K". In: *J. Phys. Chem. A* 117 (2013), pp. 8770–8781. DOI: 10.1021/jp4042183.

[35] C. Diaz, R. A. Olsen, H. F. Busnengo, and G.-J. Kroes. "Dynamics on Six-Dimensional Potential Energy Surfaces for H2/Cu(111): Corrugation Reducing Procedure versus Modified Shepard Interpolation Method and PW91 versus RPBE". In: *J. Phys. Chem. C* 114 (2010), pp. 11192–11201. DOI: 10.1021/jp1027096.

[36] W. H. Butler, F. J. Pinski, and P. B. Allen. "Phonon Linewidths and Electron-Phonon Interaction in Nb". In: *Phys. Rev. B* 19.7 (1979), pp. 3708–3721.

[37] M. J. Puska and R. M. Nieminen. "Atoms Embedded in an Electron Gas: Phase Shifts and Cross Sections". In: *Phys. Rev. B* 27 (1983), p. 6121. DOI: 10.1103/PhysRevB.27.6121.

[38] N. Gerrits, J. I. Juaristi, and J. Meyer. "Atoms in Jellium Revisited - Implications for the Local Density Friction Approximation?" In: *Prep.* (2017).

[39] P. Saalfrank, J. I. Juaristi, M. Alducin, M. Blanco-Rey, and R. D. Muiño. "Vibrational Lifetimes of Hydrogen on Lead Films: An Ab Initio Molecular Dynamics with Electronic Friction (AIMDEF) Study". In: *J. Chem. Phys.* 141 (2014), p. 234702. DOI: 10.1063/1.4903309.

[40] M. Askerka, R. J. Maurer, V. S. Batista, and J. C. Tully. "Erratum: Role of Tensorial Electronic Friction in Energy Transfer at Metal Surfaces [Phys. Rev. Lett. 116, 217601 (2016)]". In: *Phys. Rev. Lett.* 119 (2017), p. 069901. DOI: 10.1103/PhysRevLett.119.069901.

[41] C. T. Rettner, H. A. Michelsen, and D. J. Auerbach. "Quantum-State-Specific Dynamics of the Dissociative Adsorption and Associative Desorption of H_2 at a Cu(111) Surface". In: *J. Chem. Phys.* 102 (1995), pp. 4625–4641. DOI: 10.1063/1.469511.

[42] H. A. Michelsen, C. T. Rettner, D. J. Auerbach, and R. N. Zare. "Effect of Rotation on the Translational and Vibrational Energy Dependence of the Dissociative Adsorption of D_2 on Cu(111)". In: *J. Chem. Phys.* 98 (1993), pp. 8294–8307. DOI: 10.1063/1.464535.

[43] A. S. Muzas, J. I. Juaristi, M. Alducin, R. D. Muiño, G. J. Kroes, et al. "Vibrational Deexcitation and Rotational Excitation of H2 and D2 Scattered from Cu(111): Adiabatic versus Non-Adiabatic Dynamics". In: *J. Chem. Phys.* 137 (2012), p. 064707. DOI: 10.1063/1.4742907.

[44] A. C. Luntz, M. Persson, and G. O. Sitz. "Theoretical Evidence for Nonadiabatic Vibrational Deexcitation in H2(D2) State-to-State Scattering from Cu(100)". In: *J. Chem. Phys.* 124 (2006), p. 091101. DOI: 10.1063/1.2177664.

[45] K. Golibrzuch, P. R. Shirhatti, I. Rahinov, A. Kandratsenka, D. J. Auerbach, et al. "The Importance of Accurate Adiabatic Interaction Potentials for the Correct Description of Electronically Nonadiabatic Vibrational Energy Transfer: A Combined Experimental and Theoretical Study of NO($v = 3$) Collisions with a Au(111) Surface". In: *J. Chem. Phys.* 140 (2014), p. 044701. DOI: 10.1063/1.4861660.

[46] B. C. Krüger, N. Bartels, C. Bartels, A. Kandratsenka, J. C. Tully, et al. "NO Vibrational Energy Transfer on a Metal Surface: Still a Challenge to First-Principles Theory". In: *J. Phys. Chem. C* 119 (2015), pp. 3268–3272. DOI: 10.1021/acs.jpcc.5b00388.

[47] A. Hodgson, J. Moryl, P. Traversaro, and H. Zhao. "Energy Transfer and Vibrational Effects in the Dissociation and Scattering of D2 from Cu (111)". In: *Nature* 356 (1992), p. 501. DOI: 10.1038/356501a0.

[48] C. T. Rettner, D. J. Auerbach, and H. A. Michelsen. "Observation of Direct Vibrational Excitation in Collisions of H_2 and D_2 with a Cu(111) Surface". In: *Phys. Rev. Lett.* 68 (1992), pp. 2547–2550. DOI: 10.1103/PhysRevLett.68.2547.

[49] A. Hodgson, P. Samson, A. Wight, and C. Cottrell. "Rotational Excitation and Vibrational Relaxation of H 2 (Υ= 1, J= 0) Scattered from Cu (111)". In: *Phys. Rev. Lett.* 78.5 (1997), p. 963.

[50] For lower incidence energies, scattering over the top site has been found to dominate vibrational de-excitation from $\nu = 1$ in adiabatic calculations [43]. Indeed, for top sites, $\eta_{dd}^{\mathrm{ODF-iso}}$ is rather different from $\eta_{dd}^{\mathrm{LDFA}}$ so that the difference in electronic structure inherent to LDFA and ODF also becomes visible in the dynamics in this case.

[51] W. E. Perreault, N. Mukherjee, and R. N. Zare. "Preparation of a Selected High Vibrational Energy Level of Isolated Molecules". In: *J. Chem. Phys.* 145 (2016), p. 154203. DOI: 10.1063/1.4964938.

[52] S. Baroni, S. de Gironcoli, A. Dal Corso, and P. Giannozzi. "Phonons and Related Crystal Properties from Density-Functional Perturbation Theory". In: *Rev. Mod. Phys.* 73 (2001), pp. 515–562. DOI: 10.1103/RevModPhys.73.515.

[53] J. P. Perdew, J. A. Chevary, S. H. Vosko, K. A. Jackson, M. R. Pederson, et al. "Atoms, Molecules, Solids, and Surfaces: Applications of the Generalized Gradient Approximation for Exchange and Correlation". In: *Phys. Rev. B* 46 (1992), pp. 6671–6687. DOI: 10.1103/PhysRevB.46.6671.

[54] P. Giannozzi, S. Baroni, N. Bonini, M. Calandra, R. Car, et al. "QUANTUM ESPRESSO: A Modular and Open-Source Software Project for Quantum Simulations of Materials". In: *J Phys Condens Matter* 21 (2009), p. 395502. DOI: 10.1088/0953-8984/21/39/395502.

[55] D. R. Hamann. "Optimized Norm-Conserving Vanderbilt Pseudopotentials". In: *Phys. Rev. B* 88 (2013), p. 085117. DOI: 10.1103/PhysRevB.88.085117.

[56] M. Schlipf and F. Gygi. "Optimization Algorithm for the Generation of ONCV Pseudopotentials". In: *Comput. Phys. Commun.* 196 (2015), pp. 36–44. DOI: 10.1016/j.cpc.2015.05.011.

[57] J. Meyer. "Ab Initio Modeling of Energy Dissipation during Chemical Reactions at Transition Metal Surfaces". PhD thesis. Freie Universität Berlin, Freie Universität Berlin, Germany, 2012.

[58] I. Goikoetxea, J. Beltrán, J. Meyer, J. I. Juaristi, M. Alducin, et al. "Non-Adiabatic Effects during the Dissociative Adsorption of O_2 at Ag(111)? A First-Principles Divide and Conquer Study". In: *New J. Phys.* 14 (2012), p. 013050. DOI: 10.1088/1367-2630/14/1/013050.

[59] F. L. Hirshfeld. "Bonded-Atom Fragments for Describing Molecular Charge Densities". In: *Theoret. Chem. Acta* 44 (1977), pp. 129–138. DOI: 10.1007/BF00549096.

[60] J. Behler, S. Lorenz, and K. Reuter. "Representing Molecule-Surface Interactions with Symmetry-Adapted Neural Networks". In: *J. Chem. Phys.* 127 (2007), p. 014705. DOI: 10.1063/1.2746232.

[61] B. Jiang and H. Guo. "Permutation Invariant Polynomial Neural Network Approach to Fitting Potential Energy Surfaces. III. Molecule-Surface Interactions". In: *J. Chem. Phys.* 141 (2014), p. 034109. DOI: 10.1063/1.4887363.

[62] K. Shakouri, J. Behler, J. Meyer, and G.-J. Kroes. "Accurate Neural Network Description of Surface Phonons in Reactive Gas–Surface Dynamics: N_2 + Ru(0001)". In: *J. Phys. Chem. Lett.* 8 (2017), pp. 2131–2136. DOI: 10.1021/acs.jpclett.7b00784.